



# Influence of Welding Process on Microstructure and Properties of Laser Welding of SiC<sub>p</sub>/6061 Al Matrix Composite

Hongliang Li<sup>1</sup>, Hongyang Cao<sup>1</sup>, Qiang Zhu<sup>1\*</sup>, Yunbin Lu<sup>1</sup>, Zeyu Wang<sup>1</sup>, Wentao Zhao<sup>1</sup> and Hongbo Xia<sup>2\*</sup>

<sup>1</sup>School of Materials Science and Engineering, Jiangsu University, Zhenjiang, China, <sup>2</sup>College of Mechanical Engineering, Yangzhou University, Yangzhou, China

Direct laser welding, laser welding with Ti interlayer, and ultrasonic-assisted laser welding with Ti interlayer were used to join SiC<sub>p</sub>/6061 Al matrix composites. Microstructural evolutions, compositional distributions and tensile strengths under three processes were compared and analyzed. The experimental results showed that ultrasonic-assisted laser welding with Ti interlayer can obtain joints with good continuity and without obvious defects. Due to combined effects of Ti interlayer and ultrasonic, formation of brittle Al<sub>4</sub>C<sub>3</sub> phase was greatly suppressed and fine TiC precipitates were also uniformly distributed in weld metal. The strength shown by the welded joints could reach up to 77.2% of the strength of the base material. Because of the internal defects (voids and pores) and the generated large numbers of brittle phases of Al<sub>4</sub>C<sub>3</sub> in weld metal, the joint strength shown by the other two techniques, direct laser welding and laser welding with Ti interlayer, only reached 49.4 and 64.8% of the base material strength, respectively.

## OPEN ACCESS

### Edited by:

Xiangchen Meng,  
Harbin Institute of Technology, China

### Reviewed by:

Kai Feng,  
Shanghai Jiao Tong University, China  
Ting Wang,  
Harbin Institute of Technology, China

### \*Correspondence:

Qiang Zhu  
zhuqiang@ujs.edu.cn  
Hongbo Xia  
jssrxhb@126.com

### Specialty section:

This article was submitted to  
Structural Materials,  
a section of the journal  
Frontiers in Materials

**Received:** 18 September 2021

**Accepted:** 11 October 2021

**Published:** 04 November 2021

### Citation:

Li H, Cao H, Zhu Q, Lu Y, Wang Z,  
Zhao W and Xia H (2021) Influence of  
Welding Process on Microstructure  
and Properties of Laser Welding of  
SiC<sub>p</sub>/6061 Al Matrix Composite.  
Front. Mater. 8:779324.  
doi: 10.3389/fmats.2021.779324

**Keywords:** laser welding, Al matrix composite, microstructure, mechanical properties, Ti interlayer

## INTRODUCTION

Silicon carbide particles (SiC<sub>p</sub>) reinforced aluminum matrix composites (AMCs) have significant advantages such as high specific strength and specific modulus, low thermal expansion coefficient, excellent thermal conductivity and corrosion resistance. They are widely used in aerospace, aviation, ocean and automobile fields (Xie et al., 2021a; Mao et al., 2021; Xu et al., 2021). Due to the large difference in physical and mechanical properties between Al matrix and SiC<sub>p</sub>, it is a difficulty for the joining of SiC<sub>p</sub>/6061 Al matrix composites which finally narrowed its practical application.

In recent years, researchers have conducted extensive investigations on the joining of AMCs reinforced with different particles (whiskers), such as SiC, Al<sub>2</sub>O<sub>3</sub>, TiB<sub>2</sub>, B<sub>4</sub>C or ZrB<sub>2</sub> (Ellis, 1996; Xie et al., 2021b). Among them, the majority of these studies have mainly focused on the welding of SiC/Al-alloy composites. Friction stir welding is considered to be the most reliable welding method for joining of AMCs (Parikh et al., 2019; Salih et al., 2019; Kumar et al., 2020; Xie et al., 2021c). Nevertheless, friction stir welding is limited by the shape and size of the workpiece. Furthermore, high hardness of SiC particles will reduce the service life of the stirring head, which will introduce extra cost for industrial applications in large scale.

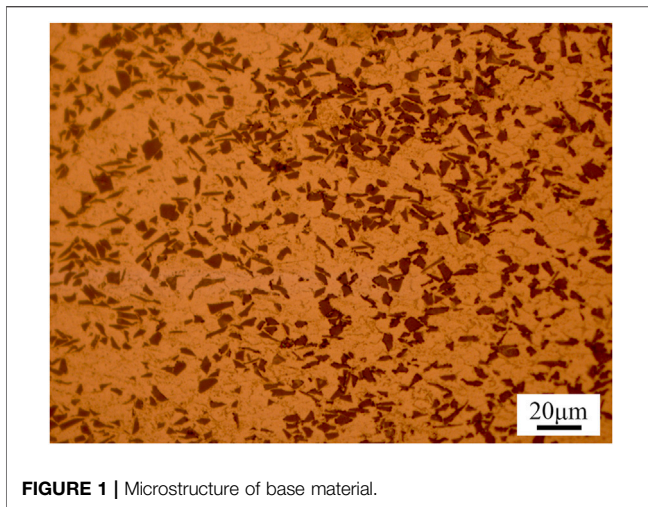


**FIGURE 1** | Microstructure of base material.

Worldwide scholars have focused on the joining of SiC<sub>p</sub>/AMCs using fusion welding such as TIG, PAW, MIG, LBW, EBW, et al. (Urena et al., 2000; García et al., 2002; Chen et al., 2006; Bassani et al., 2007; Lei et al., 2011) due to characteristics of simple equipment, strong versatility and low cost for fusion welding. However, following issues will be appeared during the fusion welding of SiC<sub>p</sub>/AMCs:

- 1) high viscosity in the molten pool
- 2) rejection of SiC particles by the solidification front
- 3) emergence of defects such as cracks, pores and low-density microstructure
- 4) weakened reinforcement effect of SiC due to the formation of brittle Al<sub>4</sub>C<sub>3</sub> compounds resulted from severe reaction between SiC with molten aluminum
- 5) high residual stresses at the Al matrix/SiC particles interface after welding thermal cycling.

As a result, the obtained SiC<sub>p</sub>/AMCs joints may have a poor appearance, severe segregation of SiC particles, and degradation of mechanical performance. Laser welding was recognized as a more ideal substitution over other traditional welding method due to its higher energy density, larger productivity and narrower heat affected zone (Chao et al., 2013; Banerjee et al., 2016). Extensive efforts have been devoted to explore the appropriate processes in order to obtain a laser welded SiC<sub>p</sub>/AMCs joints with satisfactory weld formation.

Firstly, an appropriate heat input is significant for the welding formation. For instance, Huang et al. (2001) pointed out small heat input was helpful to reduce the number of Al<sub>4</sub>C<sub>3</sub> compounds and defects which had a high consentience with previous research conducted by Bassani et al. (2007). Pulsed laser welding also had a flexible adjustment for the heat input. Yue et al. (1997) obtained a pulsed laser welded SiC<sub>p</sub>/AMCs joints with minimum defects by optimizing its laser power and pulse duration time. Generally, it is quite hard to acquire high-quality laser welded SiC<sub>p</sub>/AMCs joints by solo adjusting parameters without filler addition.

**TABLE 1** | Main parameters of laser welding process.

Process	LBW	LBW-Ti	ULBW-Ti
Laser power W		2000	
welding speed (mm·s <sup>-1</sup> )		20	
Interlayer (mm)	No	0.03Ti	0.03Ti
Ultrasonic amplitude (μm)	–	–	7.5

Secondly, active elements Si, Ti and Zr could be added into SiC-reinforced Al composites to enhance the mixing ability of the matrix and filler materials. These added alloying elements can also inhibit the interface reaction between SiC and Al, and thereby, guaranteeing the welding quality. For instance, Niu et al. (2006) suggested that the weldability of SiC<sub>p</sub>/AMCs could be improved by increasing content of Si in filler metal so as to raise activity value of Si. With the use of Ti filler, Al<sub>4</sub>C<sub>3</sub> brittle phases in laser weld joints were suppressed by the preferential generation of TiC and Ti<sub>5</sub>Si<sub>3</sub>, as demonstrated by Wang et al. (2000), Guo (2010), and Chen et al. (2002). Meanwhile, Long et al. (2020) indicated that the addition of Zr into molten pool had an excellent removal function for porosity defects and the suppression function for brittle phases.

The aforementioned researches proved the benefits of added active elements. Wang et al. (2000) pointed out that laser welding with Ti interlayer was a promising method for joining SiC<sub>p</sub>/AMCs, but no mechanical properties were covered in their research. Although the addition of active elements could improve the tensile strength of SiC<sub>p</sub>/AMCs joints, the segregation and inhomogeneous distribution of active elements would weak this effect (Guo et al. (2012)). On the other hand, fast cooling rate of laser welding process would shorten the diffusion durations of active element, which led to the segregation of active elements. Therefore, some aiding methods, such as ultrasonic or electrical stirring, could be employed to promote uniform distribution of active elements and refinement of microstructure (Yan et al., 2011; Qi et al., 2021) while this relevant research was rarely reported.

This present work intends to evaluate the feasibility of three different laser welding process for joining SiC<sub>p</sub>/AMCs, including direct laser welding, laser welding with Ti interlayer, and ultrasonic-assisted laser welding with Ti interlayer. Microstructural evolutions, elemental distributions and tensile strengths with three processes were compared and analyzed. The research of this subject can lay a foundation for laser welding of SiC<sub>p</sub>/AMCs, which has important theoretical significance and engineering application value.

## EXPERIMENTAL PROCEDURE

The Al matrix composite selected in the study was with 17 vol%, reinforcing SiC particles, which was produced by the casting method. As-received SiC<sub>p</sub>/6061Al with dimensions of 150 × 60 × 3 mm was subjected to T6 heat treatment. The microstructure of SiC<sub>p</sub>/6061Al is shown in **Figure 1**. The average particle size was 7 μm. The elemental compositions of 6061 aluminum alloy

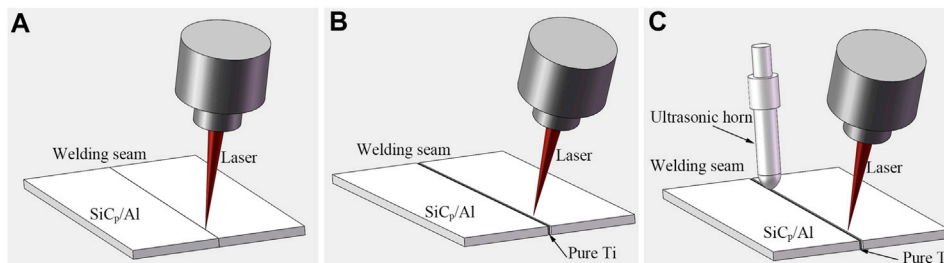


**FIGURE 2** | Schematic diagram of three welding processes: **(A)** direct laser welding **(B)** laser welding with Ti interlayer **(C)** Ultrasonic-assisted laser welding with Ti interlayer.

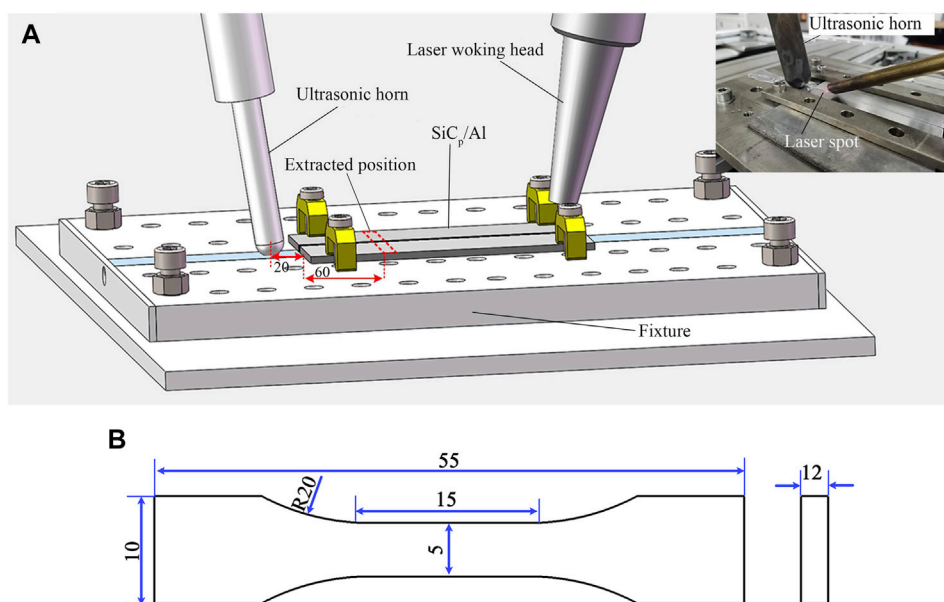


**FIGURE 3** | **(A)** The platform of ultrasonic-assisted laser welding, **(B)** the dimensions of tensile specimen (mm).

consisted of Mg-1.0, Si-0.6, Fe-0.7, Mn-0.15, Cu-0.25, Zn-0.25, Ti-0.06 and Al-Balance by wt%.

The surface of composite was firstly ground with 600 sandpaper and cleaned with ethanol before welding, and then the welding experiments was carried out immediately. The main process parameters of laser welding are shown in **Table 1**. Continuous laser mode was used in all welding trials.

**Figure 2** shows the schematic diagram of three welding processes adopted in this research, including direct laser welding (LBW), laser welding with Ti interlayer (LBW-Ti) and ultrasonic-assisted laser welding with Ti interlayer (ULBW-Ti). The purpose of active interlayer Ti and ultrasonic field were to improve the wettability and fluidity of the molten pool and reduce welding defects. The Ti interlayer with a thickness of 0.03 mm was pure Ti (Ti content was 99.99 wt%).

**Figure 3** illustrates the platform of ultrasonic-assisted laser welding, which was mainly composed of TruDisk 6002 fiber laser, ultrasonic vibration system, fixture, etc. During ultrasonic-assisted laser welding, ultrasonic was applied to the fixture and

indirectly transmitted to the workpiece. The ultrasonic horn remained fixed and the distance between the center line of the ultrasonic horn and the edge of the workpiece was 20 mm. Argon gas was selected as shielding gas with constant flow rate of 15 L/min. The defocusing distance used in laser welding process was 0 mm. The working head of laser welding carried by a KUKA robot moved to complete the welding process.

After welding, the welded joints were cut in the direction perpendicular to the weld seam to obtain metallographic and mechanical specimens. The extracted position is shown in **Figure 3A**. Stereo microscope, optical microscope and scanning electron microscope (SEM) was used to analyze the microstructural evolution of SiC<sub>p</sub>/6061Al laser welded joints. X-ray diffraction patterns (XRD) were recorded to characterize the phase constitutions of weld seam. Because laser welded joints was relatively narrow, several narrow welded joints were put together to form a large surface on which the XRD test was conducted. Tensile tests were performed on a DDL100 INSTRON 5569 universal testing machine with a displacement speed of

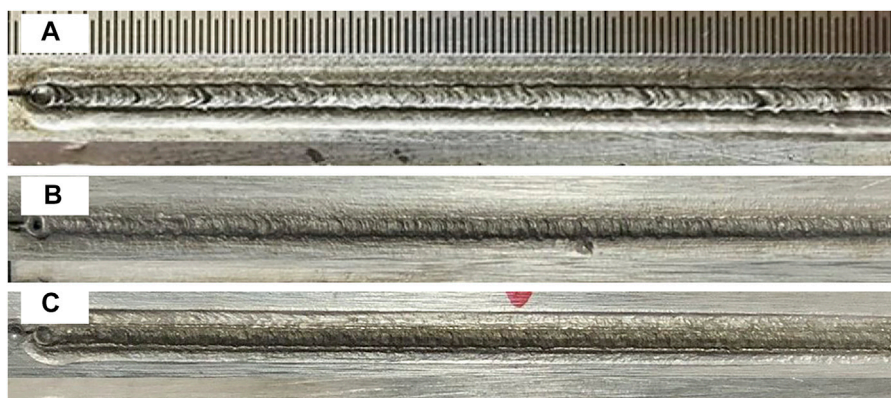


**FIGURE 4** | Surfaces morphologies of welds obtained by different welding processes, (A) direct laser welding (B) laser welding with Ti interlayer (C) Ultrasonic-assisted laser welding with Ti interlayer.

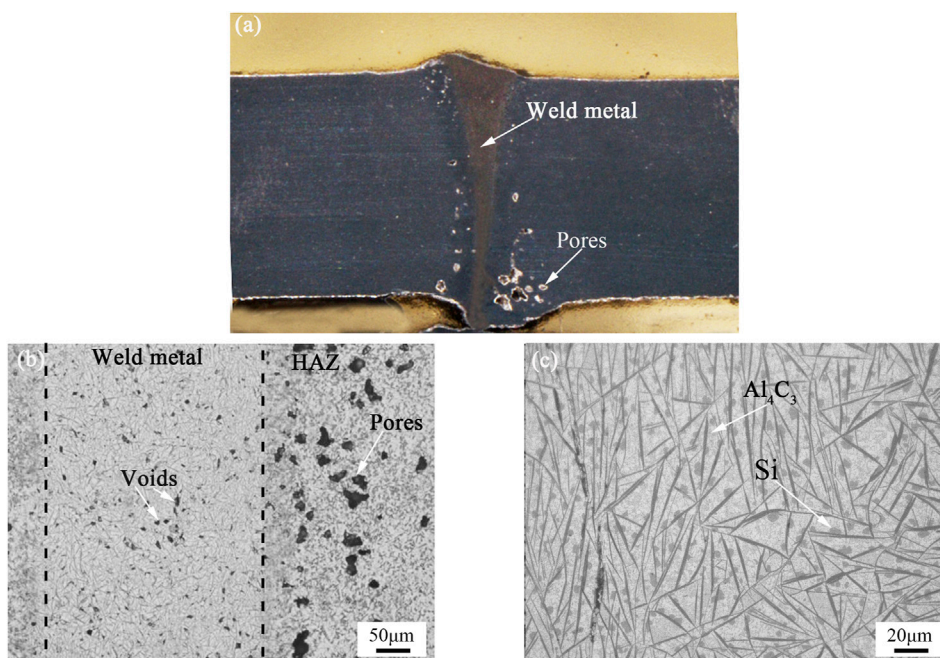


**FIGURE 5** | Cross-section and optical micrographs of SiCp/6061Al laser welded joint: (A) transverse cross section of the joint (B) microstructure of weld metal (C) enlarged view of weld metal.

1 mm/min. The specific dimensions of tensile specimen are displayed in **Figure 3B**. All the tensile results were average value of the three samples.

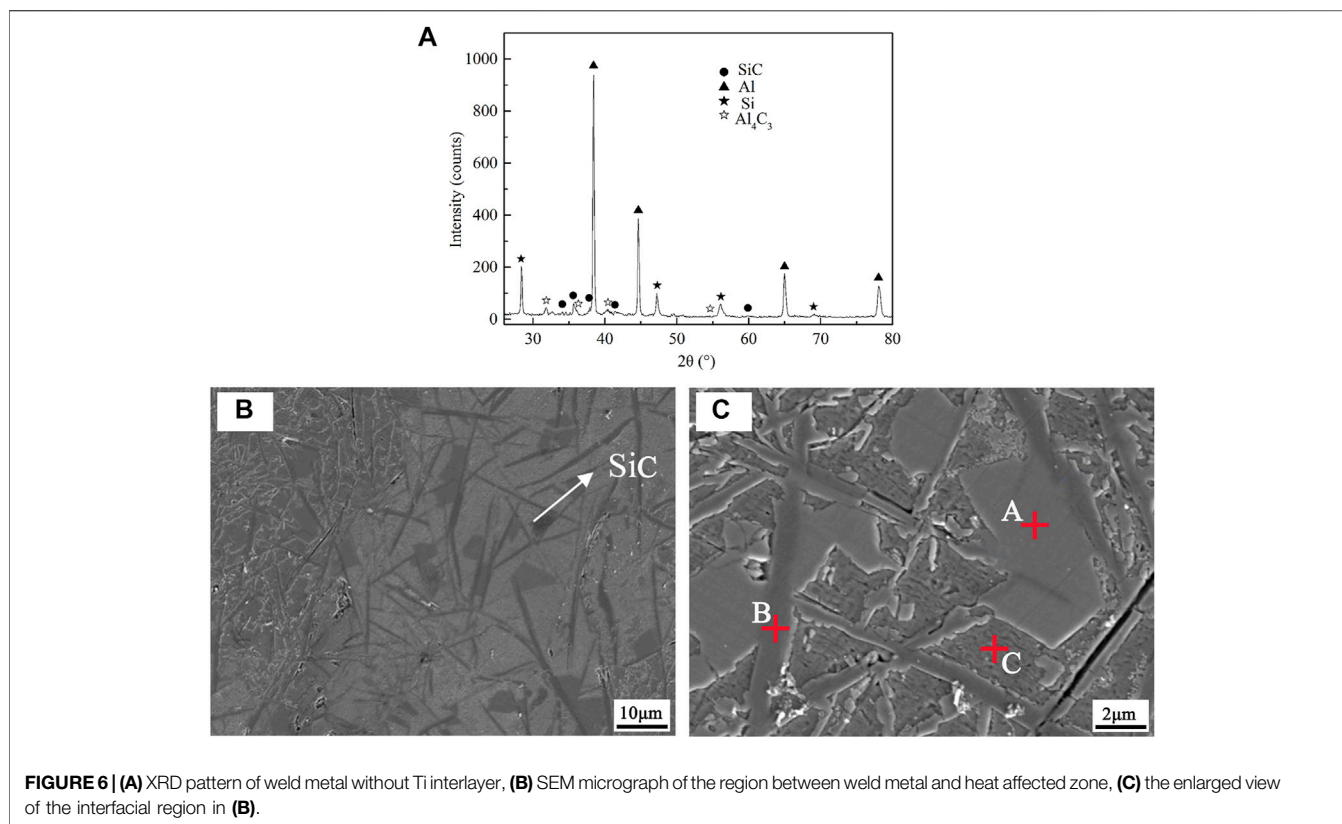
**Figure 4** display surfaces morphologies of weld appearances obtained by different welding processes. The three processes can obtain continuous welds without obvious spatters. For direct laser welding, the molten pool fluctuated violently and a rough weld surface was observed because poor wettability of SiC on Al matrix. A part of the laser energy will be consumed by Ti interlayer in the process of softening and melting. Ti also could promote the fluidity of the molten pool and reduce welding defects. Therefore, the stability of the molten pool was

improved, then a smoother weld surface was achieved for laser welding with Ti interlayer. After applying ultrasonic, the weld surface was also acceptable except shallow concavity on the surface of the weld, as shown in **Figure 4C**.

## RESULTS AND DISCUSSION

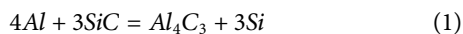
### Direct Laser Welding

**Figure 5** shows the cross-section and optical micrographs of laser welded SiCp/6061Al joint. A few pores existed in heat affected zone and some irregular shaped shrinkage voids appeared in weld



metal, which would weaken the tensile strength of the welded joint. Meanwhile, a large number of brittle needle-like  $Al_4C_3$  phases appeared in the center of the weld seam, as shown in **Figure 5C**. The length of these needlelike precipitates was in the range of 40~70  $\mu m$ . Large Si crystals were also evident in the modified composite structure. According to the chemical formula of interface reaction, the growth of  $Al_4C_3$  was usually accompanied by the precipitation of Si element.

The XRD results in **Figure 6A** demonstrated that the weld metal was mainly composed of Al matrix, Si and  $Al_4C_3$ . Only a small amount of SiC still existed in weld metal. Combined with the studies of other scholars (Yue et al., 1997; Bassani et al., 2007), the brittle needle-like phases were  $Al_4C_3$ , which was an important reason for the degradation of the tensile strength of the joint. With the increasing temperatures, the following reaction (1) occurred at the interface between Al matrix and SiC particles, which led to the formation of  $Al_4C_3$  and Si.



The reaction (1) not only consumed the reinforced phase particles (SiC) in the molten pool, but also generated brittle needle-like phase  $Al_4C_3$  which greatly reduced the mechanical properties of the welded joints. This was also consistent with the previous researches (Huang et al., 2001; Chao et al., 2013), which needed to be solved from the perspective of new process and composition regulation.

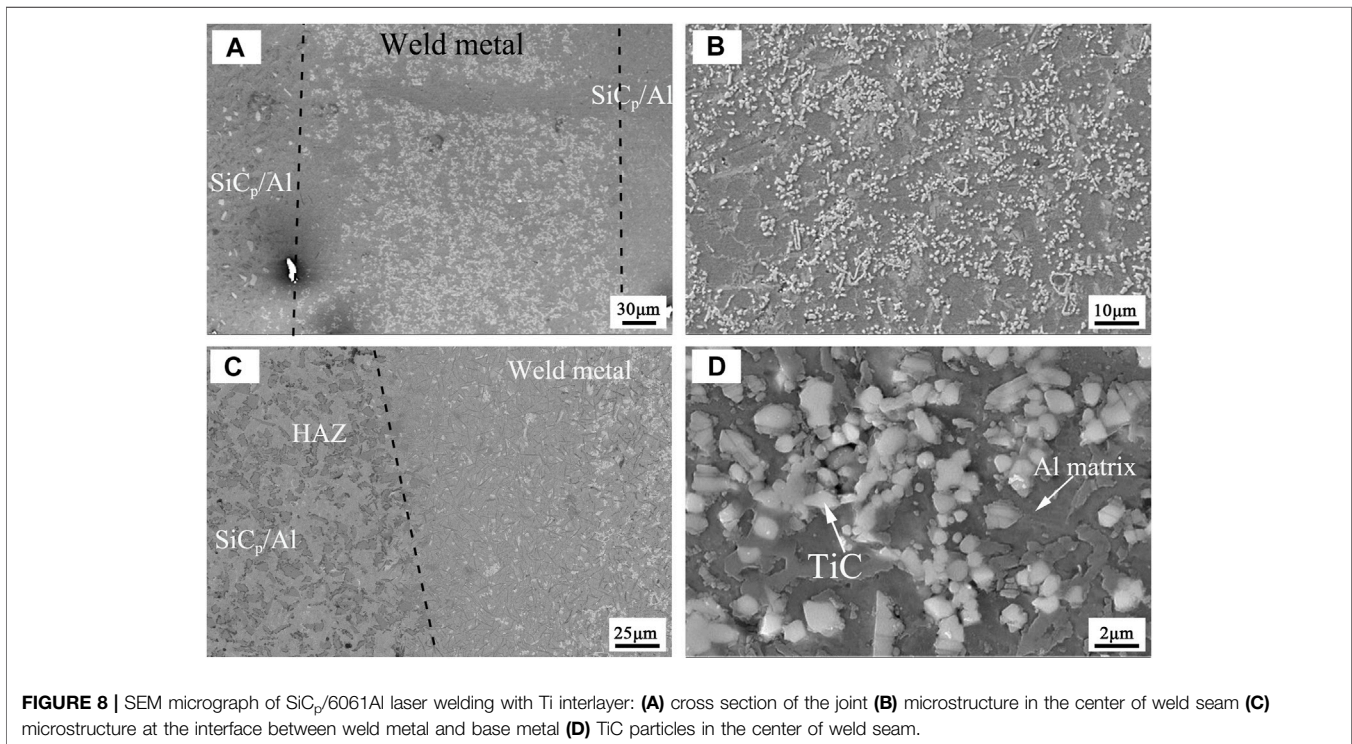
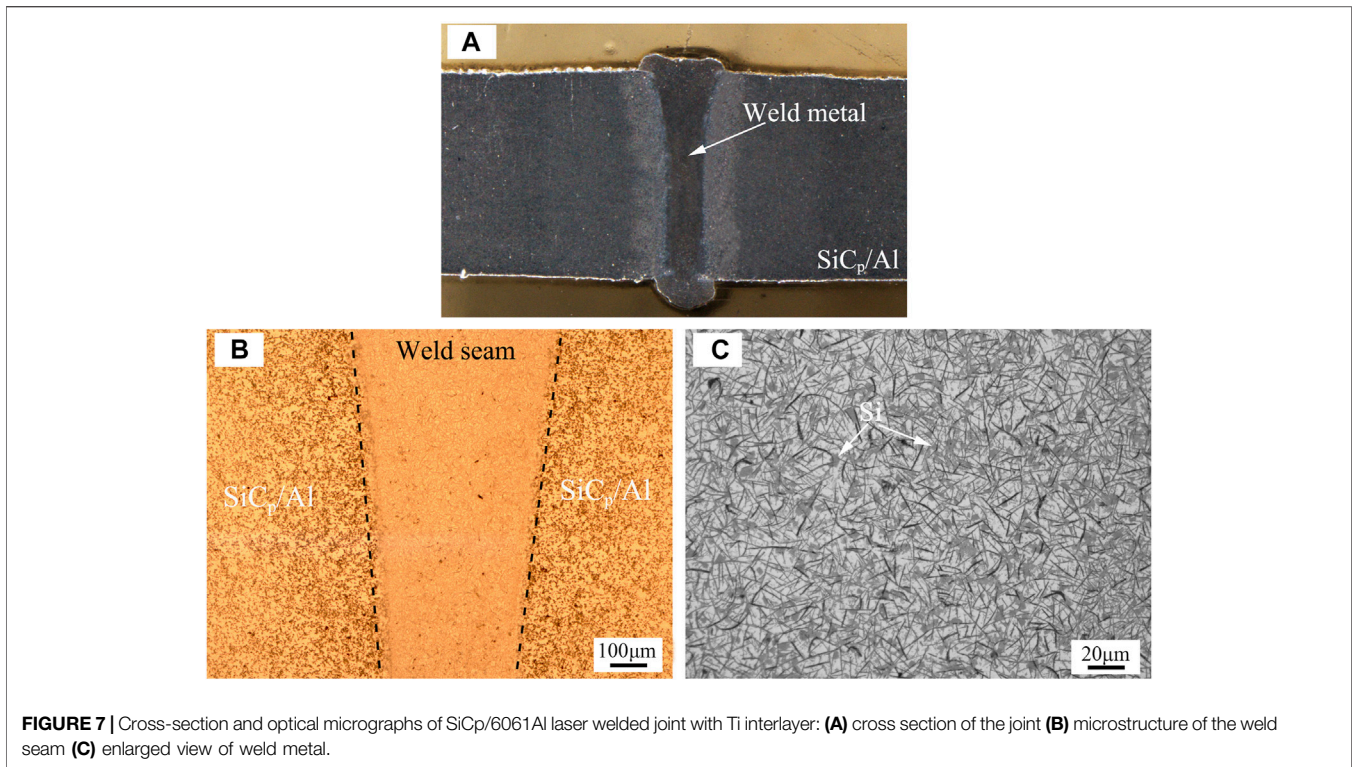
It is generally accepted that the interface reaction (1) depended on temperature and the exposure time. At high temperatures,

SiC would gradually dissolve, C elements were released from the broken Si-C covalent bonds and diffused into liquid Al, and reacted with the Al elements to form  $Al_4C_3$  precipitates. This could be verified by only few SiC particles existed in the central part of weld metal.

**Figures 6B,C** show the SEM micrograph of the region between weld metal and heat affected zone. EDX analyses were also carried out for the identification of the marked phases in **Figure 6C**. Referring to the XRD, phase A with a chemical composition of Al-2.6, C-42.1 and Si-55.3 by at% was identified as SiC. It was obvious that the SiC particles retained their original clear cut edges without any evidence of interfacial reaction phases. The chemical compositions (at%) of B and C phases were: Al-65.3, C-31.6, Si 3.1, and Al-78.1, C-7.1, Si-14.8, respectively. Therefore, these phases were recognized as  $Al_4C_3$  and Al matrix, respectively. The characterized results also indicated that  $Al_4C_3$  phases were nucleated at the surface of SiC. In addition, needle-like  $Al_4C_3$  precipitates in this region also became finer than that in the middle of weld metal where higher heat input was suffered. As clearly visualized in high magnification SEM micrographs of **Figure 6C**, the composite structure in this region was subjected to a clear variation after laser welding.

## Laser Welding With Ti Interlayer

**Figure 7** shows cross-section and optical micrographs of  $SiC_p/6061Al$  laser welded joint with Ti interlayer. As can be seen in



**Figures 7A,B**, porosity and voids defects in the welded joints almost disappeared. By comparing **Figures 5C, 7C**, the microstructures of the weld metal were significantly changed

after the addition of Ti. The distribution of acicular phases was more disordered. The length of acicular  $\text{Al}_4\text{C}_3$  phases in the weld seam was significantly reduced to about 20–30  $\mu\text{m}$ , which was

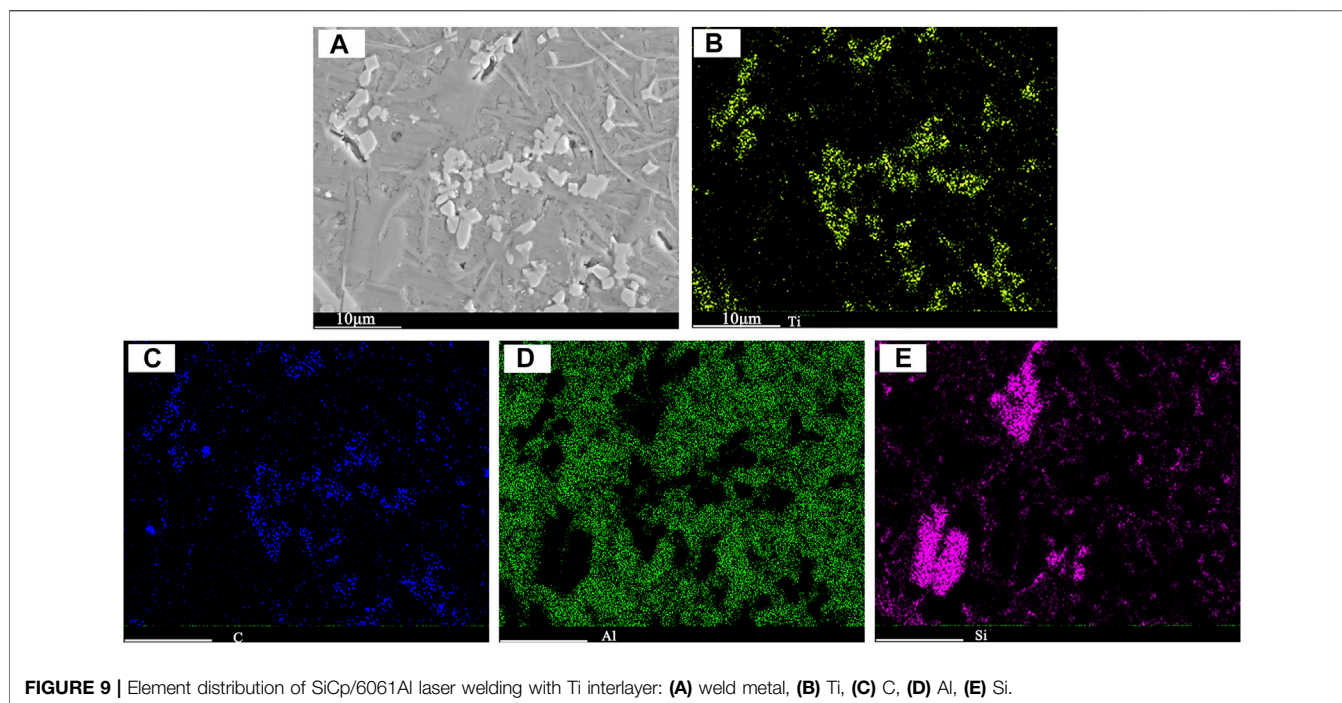


**FIGURE 9** | Element distribution of SiC<sub>p</sub>/6061Al laser welding with Ti interlayer: (A) weld metal, (B) Ti, (C) C, (D) Al, (E) Si.

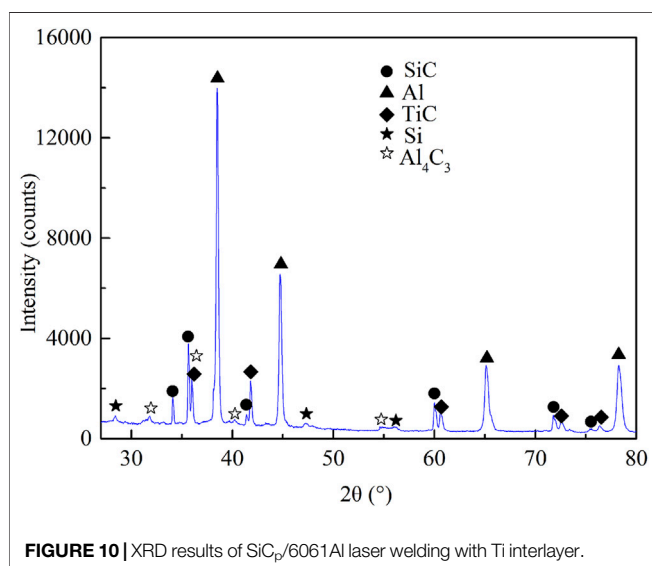


**FIGURE 10** | XRD results of SiC<sub>p</sub>/6061Al laser welding with Ti interlayer.

very important for improving the tensile strength of the welded joint. Si crystals with diameters of about 5 µm, were also evident in the modified composite structure, which was similar to that without Ti addition.

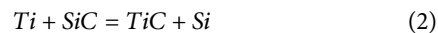
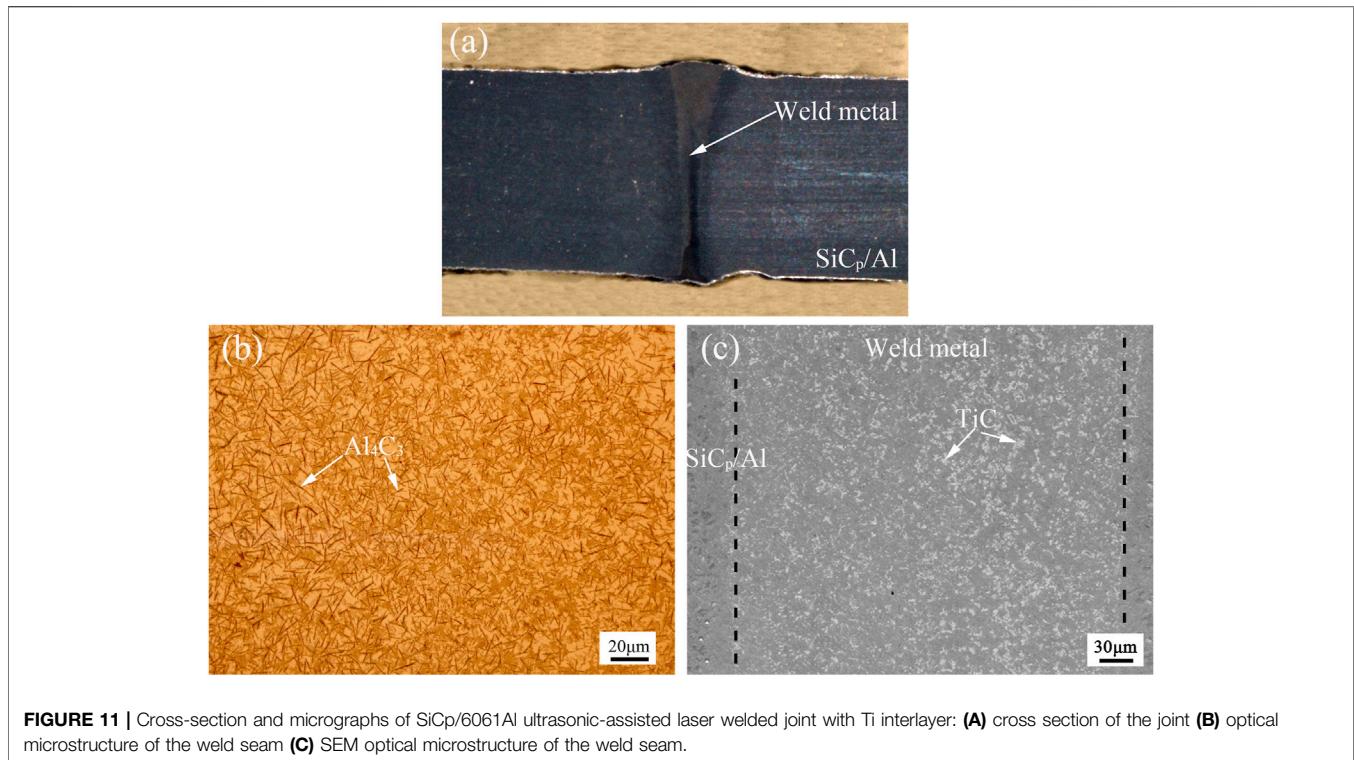
SEM micrographs of SiC<sub>p</sub>/6061Al laser welded joint with Ti interlayer at various regions with different magnifications are displayed in **Figure 8**. **Figure 8A** presents the whole welded joint with obvious interface between base metal and weld metal. The microstructure consisted of grey matrix, white particles and dark grey needlelike precipitates, as shown in **Figure 8B**. According to research by Guo (2010), the grey matrix, white particles and dark needlelike precipitates in **Figure 8C** were probably Al-Si eutectic

structures, newly formed reinforcement particle TiC and Al<sub>4</sub>C<sub>3</sub> phases, respectively.

In order to determine their element compositions, the element distribution in the typical area of weld metal was given and the measured results are as shown in **Figure 9**. It was inferred from **Figure 9A–C** that the white particles phases were mainly composed of Ti and C elements, which assumed to be the formed TiC phases. XRD results in **Figure 10** also proved this assumption. Al and Si occupied the majority of the grey matrix, as depicted in **Figures 9D,E**. It was obvious that an enrich-Si irregular phases with light grey color presented in the Al matrix. According to the research by Chen et al. (2000) and Guo et al. (2012), the addition of Ti should also cause the presence of Ti-Al and Ti-Si compounds in weld metal. However, no Ti-Al or Ti-Si compounds were detected in the present study. This was mainly due to an insufficient Ti used to react with Al and Si.

When compared **Figures 8B,C**, few needle-like Al<sub>4</sub>C<sub>3</sub> phases were observed in the central part of welded joints while it was easily formed near the fusion line due to only a small amount of Ti diffusing into this region. This made weld metal adjacent to fusion line the weakest position in the whole welded joint.

As reported by Chen et al. (2002), the affinity between Ti and C in welding process was greater than that of Al and C, which meant that Ti was easier to react with C under high temperature. Therefore, the chemical reaction (2) would take precedence over the reaction (1). Then, the formation of the Al<sub>4</sub>C<sub>3</sub> was suppressed. Instead, the newly generated white phase TiC was distributed in the weld seam. However, at a higher magnification, it was found that the TiC particles still had local segregation, and the TiC particles were not compact in combination with the Al matrix, as shown in **Figure 8D**. Furthermore, the Si formed during the reaction was distributed in Al matrix, as arrowed in **Figure 7C**.

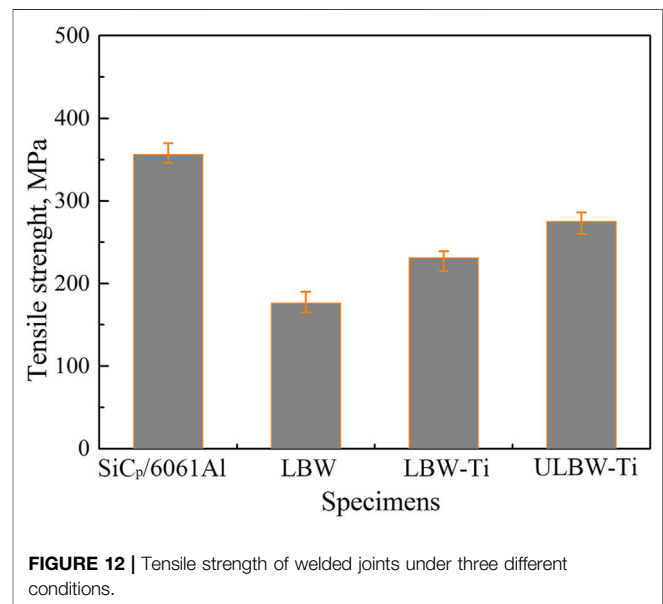


Based on the above analysis, laser welding process with Ti interlayer possessed several advantages: the addition of Ti could obviously improve the fluidity of molten pool, promote the formation of intact microstructure and reduce the number of defects such as pores and porosity. More importantly, the presence of Ti could effectively restrict the formation of  $Al_4C_3$  brittle phase, and generate in-situ TiC particles in the weld metal. Under this condition, the weld metal was transformed into Al matrix reinforced by TiC particles, granular Si crystals and some finer  $Al_4C_3$  phases. Therefore, the weldability of the material and the joint quality were improved.

### Ultrasonic-Assisted Laser Welding With Ti Interlayer

Cross-section and micrographs of SiCp/6061Al obtained by ULBW-Ti process are illustrated in **Figure 11**. It can be seen that ULAW-Ti process could also achieve welded joints without pores and crack, compared with the former two welding process. More importantly, ultrasonic vibration would promote the wetting between melt pool and base metal, which could be verified by the smooth transition of welded joints.

In addition, **Figure 11B** shows that a certain number of  $Al_4C_3$  phases with a length of 5–20  $\mu m$  still retained in the weld seam. This indicated that ultrasonic vibration did not eliminate the formation of  $Al_4C_3$  phases, but reduced the size of this needle-like phase, compared to LBW-Ti process.



Combined with the SEM micrograph in **Figure 11C**, another benefit of ultrasonic vibration on weld metal was to homogenize TiC particles. The weld metal made by LAW-Ti process contained many TiC particle clusters. More white TiC particles existed in the center of weld metal and less TiC diffused to the weld metal near the fusion line, which could not effectively limit the growth of  $Al_4C_3$ . Microstructural

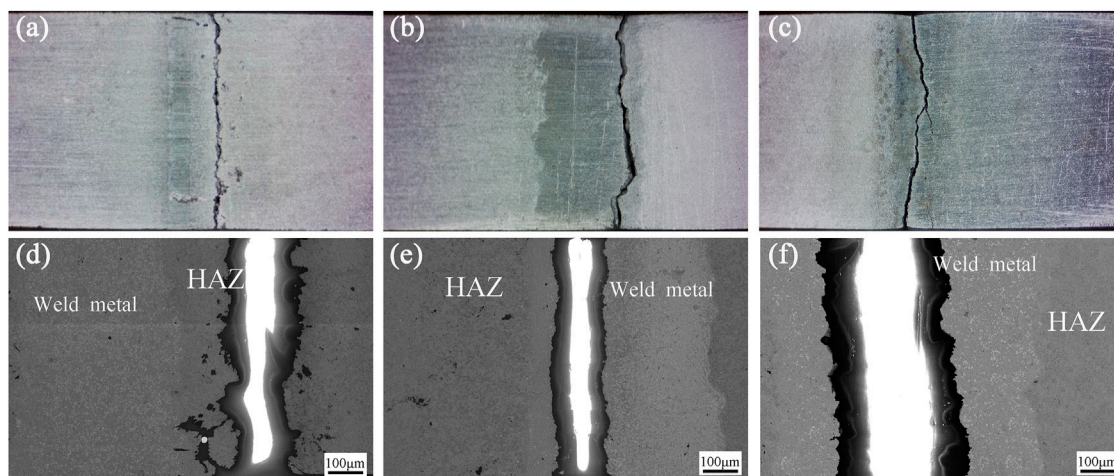


**FIGURE 13** | Fracture path of SiCp/6061Al laser welded joint: **(A,D)** laser welding, **(B,E)** laser welding Ti interlayer, **(C,F)** Ultrasonic-assisted laser welding with Ti interlayer.

heterogeneity was induced by laser welding process with Ti interlayer.

Ultrasonic vibration could stir the molten pool, thus promoting the diffusion of active Ti element in the weld metal to the periphery of the weld seam. Absence of voids and appearance of homogeneous distribution of TiC particles were more likely to achieve under the ultrasonic vibration.

### Tensile Strength of SiCp/6061Al Laser Welded Joints

The ultimate tensile strengths (UTS) of welded joints under three different welding process are shown in **Figure 12**. For laser welded joints without interlayer and ultrasonic, a joint efficiency of 49.4% was obtained. Two factors could be used to explain this low value of the tensile properties. The first was pore and voids defects presented in welded joints. The other was due to the large number of needle-like phases  $Al_4C_3$  formed in the joint during laser welding. According to the fracture path in **Figures 13A,D**, the welded joints obtained by LBW process initially fractured along the densely pores in the heat-affected zone under tensile stress. The relatively straight fracture path was almost perpendicular to the tensile direction.

For laser welding process with Ti interlayer, active element Ti improved the flowability of weld pool, which was favorable for the flotation and overflow of bubbles. The wettability between the reinforcing phase and Al matrix phase was also enhanced. This could be proved by the disappearance of pores and voids in the weld seam. In addition, heating and melting of Ti took away a part of the laser power and reduced the welding heat input on the composite. Huang et al. (2001) suggested that the size of  $Al_4C_3$  decreased with the decrease of the heat input. On the other hand, element C in the molten pool reacted preferably with Ti to generate TiC particles, as described in reaction (2). The length of  $Al_4C_3$  was significantly reduced to 10–20  $\mu m$ . The tensile strength of the joint was improved about 15% compared to

LBW process. However, the tensile strength of the joints produced by LBW-Ti process was still at a low level. This was elucidated as follows, laser welding with fast cooling rate weakened the convection stirring in the molten pool. Consequently, the diffusion ability of Ti element became poor. The newly formed TiC particles also displayed particle accumulated phenomenon to some extent. Therefore, many needle-like  $Al_4C_3$  phases formed in the weld seam near the fusion line, which produced inferior joints. **Figures 13B,E** also confirmed that the fracture occurred along the weld metal near the fusion line under tensile stress. Compared to the fracture path of LBW process, the fracture path of laser welded joint with Ti interlayer was more curved.

For ultrasonic-assisted laser welding process with Ti interlayer, the tensile strength of the joint reached up to 275 MPa, which was 77.2% that of the base metal. This suggested that the ultrasonic vibration had positive effects on microstructural evolution. According to results in **Figure 13**, needle-like  $Al_4C_3$  in the welds was further refined with the assistance of ultrasonic. Ultrasonic vibration also promoted the diffusion and migration of Ti elements in the molten pool. The formed weld metal transformed into Al matrix reinforced by dispersed TiC particle. Also, the Al matrix microstructure should be refined when ultrasonic wave was applied on the workpiece.

As depicted in **Figures 13C,F**, the fracture occurred at the center of the weld seam. The fracture path was most curved and the final fracture was at approximately  $10^\circ$  to the tensile stress, indicating that its tensile strength had been significantly improved.

**Figure 14** shows micrographs of fractured tensile specimens at different conditions. It could be found from **Figure 14A** that some pores were presented in the upper-left part of fracture surface, which reduced the load bearing capacity. Selvam et al. (2021) also stated that these pores would cause spots of accumulated stress. The result was in accordance with microstructural analysis in Part 3.1. In addition, relatively flat

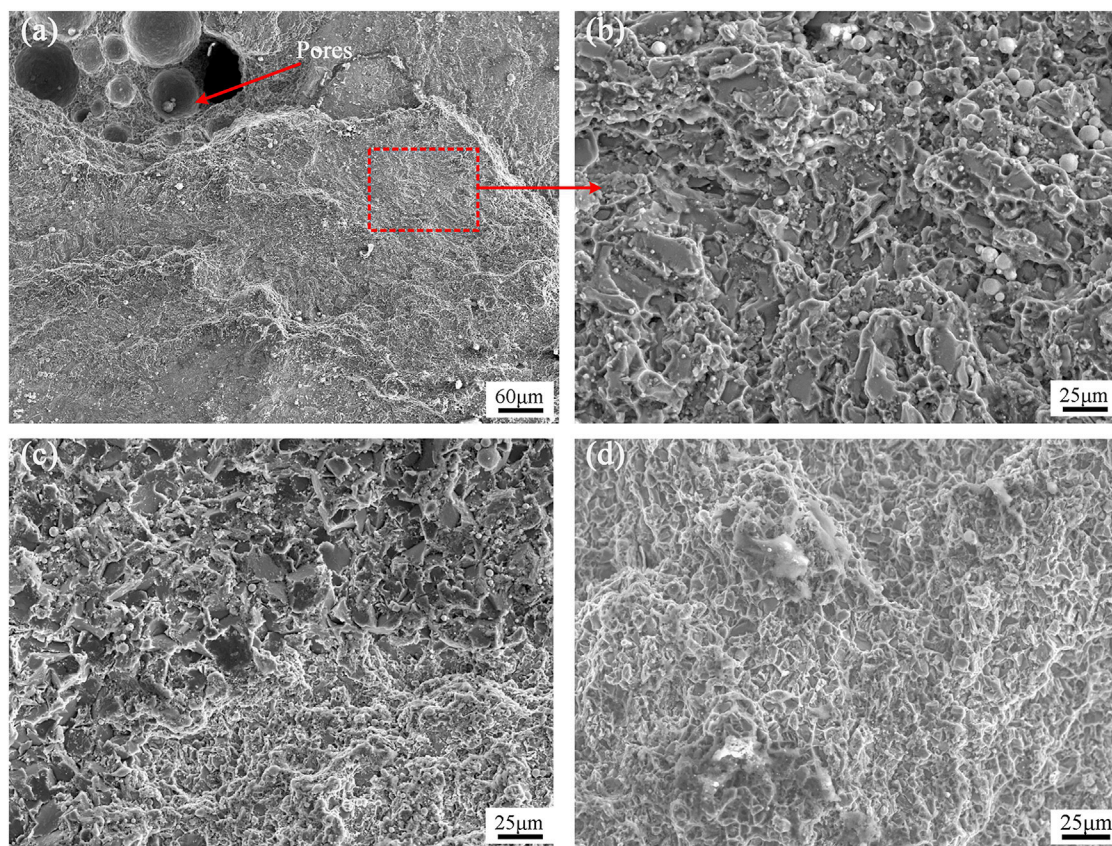


**FIGURE 14 |** Micrographs of fractured tensile specimens under three different process conditions: **(A)** direct laser welding **(B)** enlarged view of direct laser welded joint **(C)** laser welded joints with Ti interlayer **(D)** ultrasonic-assisted laser welding with Ti interlayer.

fracture surface obtained by LBW-N was obvious, indicating a brittle fracture. For fracture obtained by LBW-Ti process, many large cleavage planes were found in the fracture surface, as demonstrated in **Figure 14C**.

Compared with the first two processes, the ultrasonic-assisted laser welded joint with Ti interlayer possessed a smaller scale of cleavage planes because of reduced the size and quantity of the needle-like phases. Some dimples on the surface of the fracture were found, indicating that the joint had a certain degree of plasticity, as shown in **Figure 14D**.

## CONCLUSION

Direct laser welding, laser welding with Ti interlayer, and ultrasonic-assisted laser welding with Ti interlayer were used to joint  $\text{SiC}_p/6061$  Al matrix composites. The main conclusions were as follows:

1) Direct laser welding, laser welding with Ti interlayer and ultrasonic-assisted laser welding with Ti interlayer could obtain continuous welds. Obvious pores and voids were found in the joints produced by direct laser welding. The

weld appearances by ultrasonic-assisted laser welding with Ti interlayer was most satisfactory without any defects.

- 2) The needle-like brittle phase  $\text{Al}_4\text{C}_3$  appeared in weld metal under the three welding processes. Compared to direct laser welding and laser welding with Ti interlayer, the size of the needle-like brittle phase  $\text{Al}_4\text{C}_3$  in the ultrasonic-assisted laser weld seam structure was smaller, and the newly formed  $\text{TiC}$  was more dispersed.
- 3) By applying ultrasonic vibration and adding active element Ti, the joint efficiency of the laser welded joints with increased to 77.2%. An appropriate ultrasonic field may further improve the mechanical properties of the joints.
- 4) The main factors that influenced the tensile strength of the laser welded  $\text{SiC}_p/\text{Al}$  composites were the porosity in the welds, the absence of  $\text{SiC}$  particles in the weld metal, and the formation of brittle  $\text{Al}_4\text{C}_3$  phase.

## DATA AVAILABILITY STATEMENT

The original contributions presented in the study are included in the article/Supplementary Material, further inquiries can be directed to the corresponding authors.

## AUTHOR CONTRIBUTIONS

HL, QZ, and WZ put forward ideas, conducted experimental investigation and wrote the manuscript. HX polished the language. HC and YL contributed the guidance and supervision. ZW provided the funding. All authors have read and approved the article for publication.

## REFERENCES

- Banerjee, A. J., Biswal, M. K., Lohar, A. K., Chattopadhyay, H., and Hanumaiah, N. (2016). Review on Experimental Study of Nd:YAG Laser Beam Welding, with a Focus on Aluminium Metal Matrix Composites. *Int. J. Eng. Technol.* 5, 92–101. doi:10.14419/ijet.v5i3.5984
- Bassani, P., Capello, E., Colombo, D., Previtali, B., and Vedani, M. (2007). Effect of Process Parameters on Bead Properties of A359/SiC MMCs Welded by Laser. *Composites A: Appl. Sci. Manufacturing* 38, 1089–1098. doi:10.1016/j.compositesa.2006.04.014
- Chao, M., Cui, H., Lu, F., and Tang, X. (2013). Evolution Behavior of TiB<sub>2</sub> Particles during Laser Welding on Aluminum Metal Matrix Composites Reinforced with Particles. *T. Nonferr. Metal. Soc.* 23, 1543–1548. doi:10.1016/S1003-6326(13)62628-X
- Chen, Y. B., Zhang, D. K., Niu, J. T., and Ji, G. J. (2002). In-Situ Reinforcing Effect of Ti on Aluminum Matrix Composite during Laser Beam Welding. *Appl. Laser* 22, 320–322. doi:10.3969/j.issn.1000-372X.2002.03.015
- Chen, M.-A., Wu, C.-S., and Zou, Z.-D. (2006). Electron Beam Welding of SiCp/LD2 Composite. *Trans. Nonferrous Met. Soc. China* 16, 818–823. doi:10.1016/S1003-6326(06)60332-4
- Ellis, M. B. D. (1996). Joining of Aluminium Based Metal Matrix Composites. *Int. Mater. Rev.* 41, 41–58. doi:10.1179/imr.1996.41.2.41
- García, R., Manzano, A., López, V. H., and Bedolla, E. (2002). Comparative Welding Study of Metal Matrix Composites with the MIG Welding Process, Using Direct and Indirect Electric Arc. *Metall. Mater. Trans. B* 33, 932–937. doi:10.1007/s11663-002-0079-1
- Guo, J., Gougeon, P., and Chen, X. (2012). Study on Laser Welding of AA1100-16 vol.% B4C Metal–Matrix Composites. *Compos. Part. B-eng.* 43, 2400–2408. doi:10.1016/j.compositesb.2011.11.044
- Guo, K. W. (2010). Influence of *In Situ* Reaction on the Microstructure of SiCp/AlSi7Mg Welded by Nd:YAG Laser with Ti Filler. *J. Mater. Eng. Perform.* 19, 52–58. doi:10.1007/s11665-009-9422-x
- Huang, R. Y., Huang, J. C., and Chen, S. C. (2001). Electron and Laser Beam Welding of High Strain Rate Superplastic Al-6061/SiC Composites. *Metall. Mat. Trans. A* 32, 2575–2584. doi:10.1007/s11661-001-0047-4
- Kumar, N., Das, A., and Prasad, S. B. (2020). An Analysis of Friction Stir Welding (FSW) of Metal Matrix Composites (MMCs). *Mater. Today Proc.* 26, 2650–2656. doi:10.1016/j.matpr.2020.02.558
- Lei, Y.-C., Xue, H.-L., Hu, W.-X., Liu, Z.-Z., and Yan, J.-C. (2011). Effects of Ac Arc Ultrasonic on Plasma Arcin Situwelding of SiCp/6061Al MMCs. *Sci. Technology Welding Joining* 16, 561–566. doi:10.1179/1362171811Y.0000000030
- Long, J., Zhang, L.-J., Zhang, L.-L., Wang, X., Zhang, G.-F., Zhang, J.-X., et al. (2020). Effects of Minor Zr Addition on the Microstructure and Mechanical Properties of Laser Welded Joint of Al/SiCp Metal-Matrix Composite. *J. Manufacturing Process.* 49, 373–384. doi:10.1016/j.jmapro.2019.12.004
- Mao, D., Meng, X., Xie, Y., Yang, Y., Xu, Y., Qin, Z., et al. (2022). Strength-Ductility Balance Strategy in SiC Reinforced Aluminum Matrix Composites via Deformation-Driven Metallurgy. *J. Alloys Compounds* 891, 162078. doi:10.1016/j.jallcom.2021.162078
- Niu, J., Pan, L., Wang, M., Fu, C., and Meng, X. (2006). Research on Laser Welding of Aluminum Matrix Composite SiCw/6061. *Vacuum* 80, 1396–1399. doi:10.1016/j.vacuum.2006.01.023
- Parikh, V. K., Badgujar, A. D., and Ghetiya, N. D. (2019). Joining of Metal Matrix Composites Using Friction Stir Welding: A Review. *Mater. Manufacturing Process.* 34, 123–146. doi:10.1080/10426914.2018.1532094

## FUNDING

We are grateful for the financial support to this research from the National Natural Science Foundation of China (Grant No. 51905225) and the Postgraduate Research and Practice Innovation Program of Jiangsu Province (Grant No. SJCX20\_1400).

- Qi, L., Li, Z., Zhang, Q., Wu, W., Huang, N., and Li, Y. (2021). Electromagnetic Stirring Control for Resistance Spot Welding of SiCp/Al Composites. *J. Manufacturing Process.* 68, 1271–1279. doi:10.1016/j.jmapro.2021.06.048
- Salih, O. S., Ou, H., Wei, X., and Sun, W. (2019). Microstructure and Mechanical Properties of Friction Stir Welded AA6092/SiC Metal Matrix Composite. *Mater. Sci. Eng. A* 742, 78–88. doi:10.1016/j.msea.2018.10.116
- Selvam, J. D. R., Dinaharan, I., and Mashinini, P. M. (2021). Microstructure and Mechanical Characterization of Nd: YAG Laser Beam Welded AA6061/10wt% ZrB<sub>2</sub> Aluminum Matrix Composites. *Opt. Laser Technol.* 140, 107084. doi:10.1016/j.optlastec.2021.107084
- Ureña, A., Escalera, M. D., and Gil, L. (2000). Influence of Interface Reactions on Fracture Mechanisms in TIG Arc-Welded Aluminium Matrix Composites. *Composites Sci. Technology* 60, 613–622. doi:10.1016/S0266-3538(99)00168-2
- Wang, H. M., Chen, Y. L., and Yu, L. G. (2000). 'In-Ssitu' Weld-Alloying/Laser Beam Welding of SiCp/6061Al MMC. *Mater. Sci. Eng. A* 293, 1–6. doi:10.1016/S0921-5093(00)01249-1
- Xie, Y., Meng, X., Li, Y., Mao, D., Wan, L., and Huang, Y. (2021a). Insight into Ultra-refined Grains of Aluminum Matrix Composites via Deformation-Driven Metallurgy. *Composites Commun.* 26, 100776. doi:10.1016/j.coco.2021.100776
- Xie, Y., Meng, X., Mao, D., Qin, Z., Wan, L., and Huang, Y. (2021b). Homogeneously Dispersed Graphene Nanoplatelets as Long-Term Corrosion Inhibitors for Aluminum Matrix Composites. *ACS Appl. Mater. Inter.* 13, 32161–32174. doi:10.1021/acami.1c07148
- Xie, Y., Meng, X., Wang, F., Jiang, Y., Ma, X., Wan, L., et al. (2021c). Insight on Corrosion Behavior of Friction Stir Welded AA2219/AA2195 Joints in Astronautical Engineering. *Corrosion Sci.* 192, 109800. doi:10.1016/j.corsci.2021.109800
- Xu, B., Jiang, P., Geng, S., Wang, Y., Zhao, J., and Mi, G. (2021). In-Ssitu Reactions and Mechanical Properties of 6061 Aluminum Alloy Weld Joint with SiCp by Laser Melting Injection. *Mater. Des.* 203, 109538. doi:10.1016/j.matdes.2021.109538
- Yan, J., Xu, Z., Shi, L., Ma, X., and Yang, S. (2011). Ultrasonic Assisted Fabrication of Particle Reinforced Bonds Joining Aluminum Metal Matrix Composites. *Mater. Des.* 32, 343–347. doi:10.1016/j.matdes.2010.06.036
- Yue, T. M., Xu, J. H., and Man, H. C. (1997). Pulsed Nd-YAG Laser Welding of a SiC Particulate Reinforced Aluminium Alloy Composite. *Appl. Compos. Mater.* 4, 53–64. doi:10.1007/BF02481388

**Conflict of Interest:** The authors declare that the research was conducted in the absence of any commercial or financial relationships that could be construed as a potential conflict of interest.

**Publisher's Note:** All claims expressed in this article are solely those of the authors and do not necessarily represent those of their affiliated organizations, or those of the publisher, the editors and the reviewers. Any product that may be evaluated in this article, or claim that may be made by its manufacturer, is not guaranteed or endorsed by the publisher.

Copyright © 2021 Li, Cao, Zhu, Lu, Wang, Zhao and Xia. This is an open-access article distributed under the terms of the Creative Commons Attribution License (CC BY). The use, distribution or reproduction in other forums is permitted, provided the original author(s) and the copyright owner(s) are credited and that the original publication in this journal is cited, in accordance with accepted academic practice. No use, distribution or reproduction is permitted which does not comply with these terms.